SRTTU

JCARME
ISSN: 2228-7922
Journal of Computational and Applied Research in Mechanical Engineering
Vol. 9, No. 2, pp. 259-273
jcarme.sru.ac.ir

Numerical study of induction heating by micro / nano magnetic particles in hyperthermia

Ali Asghar Taheri and Faramarz Talati*

Faculty of Mechanical Engineering, University of Tabriz, Tabriz, Iran

Article info:

Type:	Research
Received:	04/08/2018
Revised:	05/02/2019
Accepted:	12/02/2019
Online:	20/02/2019

Keywords:
Hyperthermia,
Cancer,
Electromagnetic field,
Micro/ nanoparticles,
Bioheat equation,
Finite difference method.

Abstract

Hyperthermia is one of the first applications of nanotechnology in medicine by using micro/nano magnetic particles that act based on the heat of ferric oxide nanoparticles or quantum dots in an external alternating magnetic field. In this study, a two-dimensional model of body and tumor tissues embedded is considered. Initially, the temperature distribution is obtained with respect to tumor properties and without the presence of an electromagnetic field. Then, the effect of the electromagnetic field on the temperature distribution is studied. The results are compared with those of other papers. The results indicate that the use of the electromagnetic field causes a significant rise in the tumor temperature; however, the risk of damage to the healthy tissues surrounding the cancerous tissue seems to be high. Then, the micro/nanoparticles are injected into the tumor tissue to focus energy on cancerous tissue and maximally transfer the heat onto the tissue. The temperature distribution in the state is compared with the case with no nanoparticles and other numerical works. The results demonstrate that with the injection of nanoparticles into the tumor, the maximum temperature location is transferred to the center of the tumor and also increases to 6°C. After determining the temperature distribution in the presence of nanoparticles, the effects of different variables of the problem are studied. According to the obtained results, the increase in the concentration and radius of nanoparticles have a positive effect on the temperature distribution in the tissue; on the other hand, the increase in the frequency and size of the electrodes have a negative effect. The relevant equations are solved numerically using the finite difference method.

Nomenclature

C	Heat capacity (J/m^3K)
$\boldsymbol{E}$	Electric field strength (V/m)
f	Frequency of electromagnetic field (Hz)
N	Demagnetization factor of composite tissue
n	Concentrations of micro/nanoparticles
P_{SPM}	Heat generation rate by super-paramagnetism (W/m^3)
Q	Heat generation rate (W/m^3)
$\boldsymbol{H}$	Intensity of the magnetic field (A/m)
h_f	Apparent heat convection coefficient between the skin surface and the water (W/m^2K)
K	thermal conductivity (W/mK)
q	Direction perpendicular to the studied boundary (m)
R	Radius of the magnetic induction loop (m)
r	Radius of micro / nanoparticles (m)

*Corresponding author
Email address: talati@tabrizu.ac.ir

T	Temperature (℃)

Greek symbols

ε	Permittivity of dielectric constant ($C^2/(Nm^2)$)
η	Volume ratio of nanoparticles ($1/m^3$)
μ_0	Permeability of free space ($T.m.A^{-1}$)
σ	Conductivity (S/m)
φ	Electric potential (V)

Superscript

n	Iteration
χ	Susceptibility of magnetic nanoparticles
ω_b	Blood perfusion ($1/s$)
ω	Relaxation factor
Ω	Solution domain
Ω_h	Heating area

Subscripts

1	Normal tissues
2	Tumor tissues

1. Introduction

One of the most promising approaches in cancer therapy is hyperthermia. It is a treatment method in which the temperature of the body or local tissues increases to about 41-43°C. Various methods are employed in hyperthermia, such as the use of hot water, capacitive heating, and inductive heating of malignant cells. The possibility of treating cancer by artificially induced hyperthermia has led to the development of many different devices designed to heat malignant cells while sparing surrounding healthy tissue [1-4]. In hyperthermia, introduced to the clinical oncology a few decades ago, the cells are made sensitive for combined treatment through the use of electromagnetic energy (EM), ultrasound, etc. for a certain period of time. Hyperthermia, almost always used with other forms of cancer treatment methods, provides the synergy with different measures of the conventional treatments. In combination with radiotherapy and/or chemotherapy, hyperthermia would have higher response rates, along with improved control rate of the local tumor, better relieving effects or much better overall survival rate in selected cases of a variety of tumors [5]. In recent decades, extensive studies have been performed in the field of hyperthermia, ranging from the mechanisms of thermal cell kill to clinical trials and treatments. A series of books have been published summarizing the many experimental and clinical studies in the field of hyperthermia [6-21].

Over the last decade, the branch of hyperthermia with magnetic particles has been revived with the advent of magnetic fluid hyperthermia (MFH), where the magnetic structures used are super-paramagnetic (SPM) nanoparticles that have been suspended in water or a liquid hydrocarbon to form magnetic fluid or Ferro-fluid. It has been proved that ferrofluids and SPMs are more likely to provide useful heating than ferromagnetic (FM) particles using the low magnetic field strength. In addition, with the development of nanotechnology, embedding several metal spheres in the tissue of a tumor is not so difficult. The SPMs effectively raise the temperature of the area containing the tumor. The resulting temperature pattern is a much more uniform pattern than the pattern resulted from the heat flow using only the electromagnetic field [22]. Recently, various researchers published papers about nanofluid heat transfer [23-25].

Dughiero and Corazza simulated the induction heating of the tumor by the finite element method (FEM) and using the "Fluent" software [26]. LVet al employed micro/nanomaterials in the alive tissue using the Monte Carlo method and taking into account the pseudo-stable electromagnetic field and the unstable tissue temperature in three-dimensional tissue [22]. Sazegarnia et al. investigated hyperthermia in combination with chemotherapy mediated by gold nanoparticles and concluded that the presence of nanoparticles would increase the therapeutic efficacy [27]. Zhao et al. employed magnetic nanoparticles in hyperthermia from laboratory mice. The results indicated that the temperature of the tumor center increases significantly [28]. By the FEM, Paruch investigated the destruction of the tumor by hyperthermia by nanoparticles in the three-dimensional domain [29]. Majchrzak and Paruch examined the induction hyperthermia by considering the two-dimensional model with the BEM method [30]. Using experimental results, Nemati et al. indicated that by changing the shape of superparamagnetic particles from the spherical shape to deformed cubes (octopods),

their specific absorption rate (SAR) increases to about 70% [31]. An electroquasistatic (EQS) model of capacitive hyperthermia for treating lung tumors was proposed in [32]. Specific loss power has been measured on γ-Fe_2O_3 nanoparticles dispersed in water by means of several techniques in [33]. Joglekar et al. evaluated local heating using magnetic nanoparticle in prostatic cancer (PC3) tumors hyperthermia in vivo experiments [34]. Talati and Taheri investigated the uncertainties in induction heating by micro/ nanomagnetic articles in hyperthermia [35].

In this study, firstly the temperature distribution of tissue in the presence of a tumor and absence of nanoparticles is achieved. Then it is focused on the generation of heat by SPM. Initially, the electromagnetic field is solved with inhomogeneous boundary conditions. Then the two-dimensional bio-heat equation is solved. The temperature distribution of tissue in the presence and absence of nanoparticles is analyzed and compared with each other. The effects of changes in all variables in magnetic hyperthermia are studied in this paper.

In selecting the magnetic particles, iron oxides of magnetite Fe_2O_3 and maghemite γ-Fe_2O_3 have been much studied due to having magnetic properties and biological compatibility. The magnetic oxides heating by using an alternating magnetic field mainly depend on both waste reorientation of magnetization or frictional dissipation process (if the particle is able to rotate in a small enough viscous environment). The particles used in magnetic hyperthermia must be small enough, and the frequency of alternating field to produce every significant eddy or Foucault current needs to be very low as well [22].

To obtain the potential distribution inside the tissue and temperature distribution, the Laplace and famous Pennes equations are used, respectively. Pennes equation provides acceptable results for such analyses. The finite difference method is used to solve these equations. Due to the simplicity of the finite difference method in simple geometry analysis, it has many various applications in solving problems [36-41].

2. Theoretical models and the solutions

Similar to the previous work of the authors, a rectangular area with dimensions of 0.08 × 0.04 m is considered. The heating area by electrodes (Ω_h) is limited to {0.032 m ≤ x ≤ 0.048 m, y = 0} and {0.032 m ≤ x ≤ 0.048 m, y = 0.04 m} and the area Ω = {0.032 m ≤ x ≤ 0.048 m, 0.016 m ≤ y ≤ 0.032 m} as shown in Fig. 1, represents the tumor area [35]. To prevent damage caused by overheating to the surface of the skin, these surfaces are cooled by two cooling pads put on the surface of the skin.

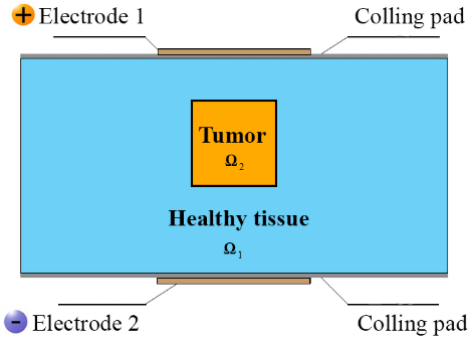

Fig. 1. The area of tissue and tumor in the two-dimensional model.

2.1. Electromagnetic field model

To generate heat in biological tissues by applying an external electromagnetic field, primarily, the two-dimensional quasi-stationary electromagnetic field induced by two plate electrodes should be numerically evaluated. The potential inside the tissue (φ) is obtained by solving the Laplace equation [22]:

$$\nabla.[\varepsilon(x,y).\nabla\varphi(x,y)] = 0\,. \qquad (1)$$

where $\varepsilon\ (x,\ y)$ is the permittivity dielectric constant of the tissue. The boundary conditions of the Eq. (1) for tissue boundaries can be stated as follows [22]:

$$\begin{aligned} &\varphi(x,y) = \pm U && (x,y) \in \Omega_h\,, \\ &\frac{\partial\varphi(x,y)}{\partial q} = 0 && (x,y) \notin \Omega_h\,. \end{aligned} \qquad (2)$$

where Ω_h and U are the electrode scope (heating area) and the electric potential difference applied on electrodes respectively, and q is direction

perpendicular to the studied boundary. The following conditions should be met at the contact surface of normal and tumor tissues [22]:

$$\varphi_1(x,y) = \varphi_2(x,y)\,,\quad \varepsilon_1 \frac{\partial \varphi_1(x,y)}{\partial q} = \varepsilon_2 \frac{\partial \varphi_2(x,y)}{\partial q}. \tag{3}$$

where ε_1 is the permittivity of the dielectric constant of healthy tissue, ε_2 is the permittivity of the dielectric constant of the tumor, φ_1 and φ_2 are the electric potential of healthy tissue and tumor, respectively. The electric field strength is obtained from the following equation:

$$\boldsymbol{E}(x,y) = -\nabla\varphi(x,y). \tag{4}$$

The intensity of the magnetic field can be expressed as follows [22]:

$$|\boldsymbol{H}(x,y)| = \frac{1}{1+N(\chi)} \frac{|\boldsymbol{E}(x,y)|}{\mu_0 \pi f R}. \tag{5}$$

where μ_0 is the dielectric constant of free space permeability ($\mu_0 = 4\pi \times 10^{-7}\, T.m.A^{-1}$), f is the frequency of the electromagnetic field, R is the radius of the magnetic induction loop, $N(\chi) = 1/3$ (for spherical composite) is the demagnetization factor of composite tissue, and χ is the susceptibility of magnetic nanoparticle.
For the small field and assuming minimal interaction between the particles forming the SPMs, the ferrofluid magnetization response (a combination of ferromagnetic materials and liquid that are highly magnetic in the presence of a magnetic field) under an alternating field can be expressed as a statement of its hybrid components: $\chi = \chi' + i\chi''$; both χ' and χ'' components are dependent on the frequency. The heat generated by the super magnet is obtained by the following equation [22]:

$$P_{SPM} = \mu_0 \pi f \chi'' |\boldsymbol{H}|^2. \tag{6}$$

The heat generated (Q_{r1}) due to the power dissipation of the electromagnetic field is dependent on the conductivity of healthy tissue (σ_1) and the strength of the electric field ($\boldsymbol{E}$). Therefore, the volumetric heat can be almost obtained as below by using the Eq. (4) for the electric field of ($\boldsymbol{E}$) [22]:

$$Q_{r1} = \sigma_1 \frac{|\boldsymbol{E}(x,y)|^2}{2} = \frac{\sigma_1 \left[|E_x|^2 + |E_y|^2\right]}{2}. \tag{7}$$

The heat generated in the tumor tissue due to the induction of SPM by EM field can be calculated by the following equation [22]:

$$Q_{r2} = \frac{1}{\Delta V}\left[\frac{4}{3} n \Delta V\, P_{SPM} \pi r^3 + \left(\Delta V - \frac{4}{3} n \Delta V \pi r^3\right)\frac{\tilde{\sigma}}{2}\right] |\boldsymbol{E}(x,y) = \left[\frac{3\pi r^3 \chi''}{4\mu_0 f R^2} + (1-\eta)\frac{\tilde{\sigma}}{2}\right].\left[|E_x|^2 + |E_y|^2\right]. \tag{8}$$

where $\tilde{\sigma}$ is the effective electrical conductivity in tumor tissue, $\eta = 4\pi n r^3/3$ is the SPM volume ratio in the tissue, r is the radius of SPM micro/ nanoparticles, n the concentrations of SPM micro/ nanoparticles, and ΔV is the control volume of the tumor tissue.

2.2 Thermal model

The famous Pennes equation is used for the heat model of biological tissues. As already mentioned, despite the simplicity, this equation provides acceptable results for such analyses. Assuming that the coefficient of thermal conductivity is variable, the Pennes equation would be rewritten as follows [42]:

$$C \frac{\partial T(x,y,t)}{\partial t} = \nabla.\left(K(x,y)\nabla T(x,y,t)\right) - \omega_b(x,y) C_b T(x,y,t) + Q(x,y,t), \quad (x,y) \in \Omega\,. \tag{9}$$

where Ω is the solution domain, $Q(x,y,t) = \omega_b(x,y) C_b T_a + Q_m(x,y,t) + Q_r(x,y,t)$, C is the heat capacity of tissue, C_b is the heat capacity of blood, T_a is the temperature of the supplier artery that assumed to be constant, T is the tissue temperature, K is the thermal conductivity (space dependent), ω_b is the blood perfusion of the location function, Q_m is the heat generation (space dependent) resulting from body metabolism, and Q_r is the heat source of heat generation dependent on location.
The above equation is used for tissues without SPM. The equation needs to be revised for tissues with injected SPM according to the

effective capacity method. The Eq. (9) can be written as follows [42]:

$$\begin{matrix}\tilde{C}\frac{\partial T(x,y,t)}{\partial t} = \nabla.\left(\tilde{K}(x,y)\nabla T(x,y,t)\right) \\ -\omega_b(x,y)C_bT(x,y,t) + Q(x,y,t), \qquad (x,y) \in \Omega\,.\end{matrix} \tag{10}$$

where $\tilde{C}$ is the effective heat capacity and $\tilde{K}$ is the effective thermal conductivity. The target area is assumed to be homogeneous in the tumor area. The thermophysical properties of cancerous tissue filled with SPM can be obtained approximately through the sequential arrangement of the relevant volume ratio of each substance [42]:

$$\tilde{C} = (1-\eta)C_2 + \eta C_3(x,y) \in \Omega_2\,, \tag{11}$$

$$\tilde{K} = ((1-\eta)/K_2 + \eta/K_3)^{-1}(x,y) \in \Omega_2\,, \tag{12}$$

$$\tilde{\sigma} = ((1-\eta)/\sigma_2 + \eta/\sigma_3)^{-1}(x,y) \in \Omega_2. \tag{13}$$

where C_2 is the heat capacity of the tumor tissue, C_3 is the heat capacity of SPM nanoparticles, K_2 is the thermal conductivity of the tumor tissue, K_3 is the thermal conductivity of SPM nanoparticles, σ_2 is the electrical conductivity of the tumor tissue, and σ_3 is the electrical conductivity of SPM nanoparticles.

Assuming stable conditions and that the values of $\tilde{K}, \omega_b \text{ and } Q_m$ in each tumor and normal areas are constant, the Eq. (10) is turned as follows for each of these areas [42]:

$$\begin{matrix}\tilde{K}\nabla^2T(x,y) - \omega_bC_bT(x,y) \\ + \omega_bC_bT_a \\ +Q_m + Q_r(x,y) = 0 \qquad (x,y) \\ \in \Omega\,.\end{matrix} \tag{14}$$

where the values of $\tilde{K}$, ω_b and Q_m are determined depending on the studied region. The boundary conditions of Eq. (14) are defined as [42]:

$$\begin{matrix}-\tilde{K}\frac{\partial T}{\partial y} = h_f(T_f - T), \\ at\ (x = 0\ and\ x = 0.08\,m;\ 0 \le y \le 0.04\,m), \\ -\tilde{K}\frac{\partial T}{\partial y} = 0, \\ at\ (0 \le x \le 0.08\,m;\ y = 0\ and\ y = 0.04\,m).\end{matrix} \tag{15}$$

where h_f is the apparent heat convection coefficient between the skin surface and water, and T_f is the initial temperature of the water. The reason for selecting adiabatic conditions for boundaries in the y-direction is that in places away from the target area, the temperature field is not almost affected by the district center or external heating or cooling. The following conditions should be met at the contact surface of normal tissues and the tumor [42]:

$$\begin{matrix}T_1(x,y) = T_2(x,y)\,, \\ K_1\frac{\partial T_1(x,y)}{\partial q} = K_2\frac{\partial T_2(x,y)}{\partial q}\,.\end{matrix} \tag{16}$$

where K_1 is the thermal conductivity of healthy tissue, K_2 is the thermal conductivity of tumor, T_1 is the healthy tissue temperature, and T_2 is the tumor temperature.

3. Discretization of equations

3.1 Potential equation

In this section, all presented equations in this paper are discretized in accordance with the Ref. [43]. In the case of equation related to the tissue potential, the Eq. (1) is rewritten as follows for each of tumor and healthy areas because of constant dielectric constant:

$$\nabla^2\varphi(x,y) = \frac{\partial^2\varphi}{\partial x^2} + \frac{\partial^2\varphi}{\partial y^2} = 0\,. \tag{17}$$

by choosing $\Delta x = \Delta y$ and using the relaxation factor, the above equation is discretized as follows with the second-order error:

$$\varphi_{i,j}^{\overline{n+1}} = \left(\varphi_{i+1,j}^n + \varphi_{i-1,j}^n + \varphi_{i,j+1}^n + \varphi_{i,j-1}^n\right)/4\,. \tag{18.a}$$

$$\varphi_{i,j}^{n+1} = \omega\varphi_{i,j}^{\overline{n+1}} + (1-\omega)\varphi_{i,j}^n. \tag{18.b}$$

in the above equation, *n* represents the iteration and ω is the relaxation factor that its value is obtained through trial and error method. The value of $\varphi_{i,j}^{\overline{n+1}}$ is obtained from Eq. (18.a) and replaced in Eq. (18.b). The use of a relaxation factor accelerates the convergence. If ω> 1, the above method is called a Successive Over-Relaxation (SOR) method, if ω< 1, it would be called as Successive Under-Relaxation (SUR), and if ω = 1, this method is converted to Gauss–Seidel method.

The equations related to contact surface of the tumor and healthy tissue (Eq. (3)) turn as follows after discretization:

$$\begin{aligned}
&\varphi^n_{X1,j} = \left(\varepsilon_2\varphi^n_{X1+1,j} + \varepsilon_1\varphi^n_{X1-1,j}\right)/(\varepsilon_1+\varepsilon_2),\\
&\varphi^n_{X2,j} = \left(\varepsilon_1\varphi^n_{X2+1,j} + \varepsilon_2\varphi^n_{X2-1,j}\right)/(\varepsilon_1+\varepsilon_2),\\
&\varphi^n_{i,Y1} = \left(\varepsilon_2\varphi^n_{i,Y1+1} + \varepsilon_1\varphi^n_{i,Y1-1}\right)/(\varepsilon_1+\varepsilon_2),\\
&\varphi^n_{i,Y2} = \left(\varepsilon_1\varphi^n_{i,Y2+1} + \varepsilon_2\varphi^n_{i,Y2-1}\right)/(\varepsilon_1+\varepsilon_2).
\end{aligned} \tag{19}$$

where *X1*, *X2*, *Y1*, and *Y2* indicate the region of the tumor. The boundary conditions of Eq. (1), i.e., Eq. (2), are discretized as follows:

$$\begin{aligned}
&\varphi_{i,1} = -U && in \quad (x \in \Omega_h, y = 0\ m),\\
&\varphi_{i,1} = \varphi_{i,2} && in \quad (x \notin \Omega_h, y = 0\ m),\\
&\varphi_{i,N} = +U && in \quad (x \in \Omega_h, y = 0.04\ m),\\
&\varphi_{i,N} = \varphi_{i,N-1} && in \quad (x \notin \Omega_h, y = 0.04\ m),\\
&\varphi_{1,j} = \varphi_{2,j} && in \quad (x = 0\ m, y),\\
&\varphi_{M,j} = \varphi_{M-1,j} && in \quad (x = 0.08\ m, y).
\end{aligned} \tag{20}$$

Eq. (4), which represents the electric field strength, is converted as follows after leading discretization and error of the first order:

$$E_{i,j} = -\left(\frac{\varphi_{i+1,j} - \varphi_{i,j}}{\Delta x}, \frac{\varphi_{i,j+1} - \varphi_{i,j}}{\Delta y}\right). \tag{21}$$

Assuming $\Delta x = \Delta y$, the squared size of the electric field with second-order error is obtained by the following equation:

$$|E_{i,j}|^2 = \left[\left(\varphi_{i+1,j} - \varphi_{i,j}\right)^2 + \left(\varphi_{i,j+1} - \varphi_{i,j}\right)^2\right]/\Delta x^2. \tag{22}$$

3.2 Bioheat equation

Pennes bioheat equation, Eq. (14), is discretized with the second-order error as follows:

$$\begin{aligned}
&T^{\overline{n+1}}_{i,j} = (T^n_{i+1,j} + T^n_{i-1,j} + T^n_{i,j+1} + T^n_{i,j-1}\\
&+\frac{\Delta x^2}{\tilde{K}}\left(\omega_b C_b T_a + Q_m + Q_{ri,j}\right))/\left(4 + \frac{\Delta x^2}{\tilde{K}}\omega_b C_b\right). && (23.a)\\
&T^{n+1}_{i,j} = \omega T^{\overline{n+1}}_{i,j} + (1-\omega)T^n_{i,j}\,. && (23.b)
\end{aligned}$$

in the above equation, n indicates the iteration and ω is the relaxation factor, that its value comes from the trial and error method. The boundary conditions of Eq. (14), i.e., Eq. (15), will be as follows after discretization:

$$\begin{aligned}
&T^n_{i,1} = \left(h_f.\Delta x.T_f/\tilde{K} + T^n_{i,2}\right)/\left(1 + h_f.\Delta x.T_f/\tilde{K}\right),\\
&T^n_{i,N} = \left(h_f.\Delta x.T_f/\tilde{K} + T^n_{i,N-1}\right)/\left(1 + h_f.\Delta x.T_f/\tilde{K}\right),\\
&T^n_{1,j} = T^n_{2,j},\\
&T^n_{M,j} = T^n_{M-1,j}.
\end{aligned} \tag{24}$$

Also, the following conditions should be met at the surface contact of healthy tissue and the tumor:

$$\begin{aligned}
&T^n_{X1,j} = \left(K_2 T^n_{X1+1,j} + K_1 T^n_{X1-1,j}\right)/(K_1+K_2),\\
&T^n_{X2,j} = \left(K_1 T^n_{X2+1,j} + K_2 T^n_{X2-1,j}\right)/(K_1+K_2),\\
&T^n_{i,Y1} = \left(K_2 T^n_{i,Y1+1} + K_1 T^n_{i,Y1-1}\right)/(K_1+K_2),\\
&T^n_{i,Y2} = \left(K_1 T^n_{i,Y2+1} + K_2 T^n_{i,Y2-1}\right)/(K_1+K_2).
\end{aligned} \tag{25}$$

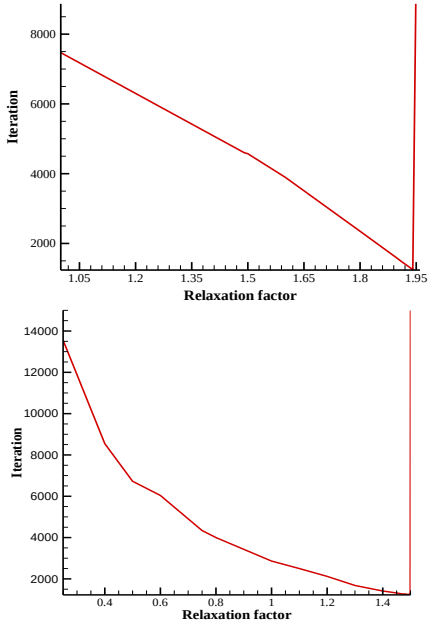

Fig. 2. Changes in the number of iterations per changes in the relaxation factor; determining the relaxation factor in (a) potential equation and (b) bioheat equation.

4. Numerical solution

The solution domain is a rectangle with the size of $0.08\,m \times 0.04\,m$. Selecting $\Delta x = \Delta y = 0.0008\,m$, the number of compute nodes along the *x* and *y* axes would be respectively equal to $M = 0.08/\Delta x + 1 = 101$ and $N = 0.04/\Delta x + 1 = 51$. Also to evaluate the grid independency, $\Delta x = \Delta y = 0.001\,m$ is considered, which corresponds to $M = 81$ and $N = 41$. Fig. 2 shows the iteration changes versus the relaxation factor in the calculations and for $\Delta x = \Delta y =$

0.0008 m. According to Fig. 2, the optimal value of relaxation factor is determined for the equation related to potential of ω= 1.9399 and for the equation related to bioheat equation of ω= 1.4981.

The mean absolute error of calculation in each iteration is calculated in accordance with the following equation [43]:

$$\varepsilon^n = \frac{\sum_{i=1}^{M}\sum_{j=1}^{N}|\varphi^{n+1} - \varphi^n|}{M \times N}. \quad (26)$$

where *n* represents the iteration. If the amount of error becomes less than the convergence criterion assumed here equal to 10^{-6}, the calculation is stopped. Fig. 3 shows the changes occurring in the error from the start to finish of the iterations for $\Delta x = \Delta y = 0.0008\, m$.

Due to the importance of temperature distribution in this study, the grid independence was examined on this variable. Fig. 4 shows this independence of the network for three value of the grid size and the same inputs ($U = 8\, V, f = 1\, MHz, r = 10\, nm, n = 1E19, \chi'' = 18, h_f = 45\ W/(m^2K), T_f = 20$ ℃). As can be seen, these figures are in agreement with each other and independent from the grid.

5. **Results and discussion**

5.1 Model without paramagnetic nanoparticle

First, the temperature distribution of the whole area is calculated without applying the electromagnetic field.

The following values are assumed for the healthy tissue; thermal conductivity: $K_1 = 0.5\ [W/mK]$, blood perfusion rate: $\omega_{b1} = 0.0005\ [1/s]$, metabolic thermal source: $Q_{m1} = 4200\ [W/m^3]$, blood temperature: $T_a = 37$ ℃, and blood heat capacity: $C_b = 4.2\ [MJ/m^3K]$. It has been proven that the presence of a malignant tumor in the tissue can cause very different blood perfusion as well as abnormal heat capacity and metabolism heat in the tumor area. The following values are related to the tumor on the skin and filled with vessels; thermal conductivity factor: $K_2 = 0.6\ [W/mK]$, blood perfusion rate: $\omega_{b2} = 0.002\ [1/s]$, and metabolic thermal source: $Q_{m2} = 42000\ [W/m^3]$. Two types of boundary conditions on the surface of the skin are considered. In the first type, the constant temperature of $T_c = 32.5$℃ is assumed. In the latter case, the third type condition with heat convection coefficient of $h_f = 45\ [W/(m^2K)]$ and temperature of $T_f = 20$ ℃ are considered.

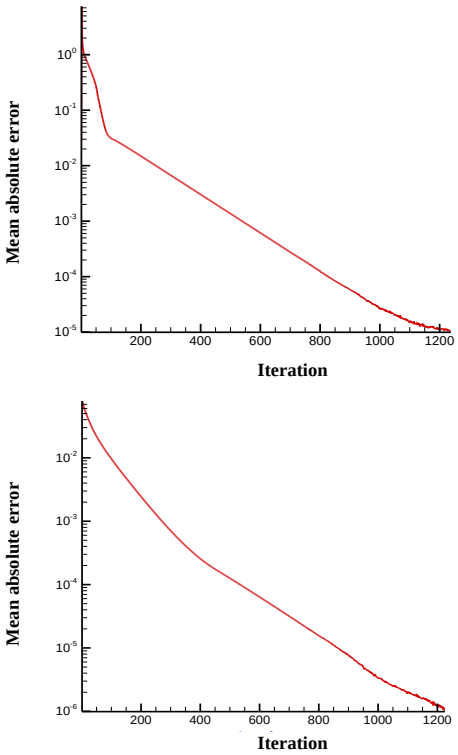

Fig. 3. Mean absolute error in each iteration and its convergence; (a) Potential equation error and (b) Bioheat equation error.

The adiabatic assumption is considered for other boundary conditions. The maximum temperature in two modes is respectively as 38.129℃ and 38.44℃. Figs. 5 and 6 show the temperature distribution in the two cases. The black square shape represents the tumor area. The aim of this study was to determine the values of the electromagnetic field, causing the temperature to reach over 42℃. The input data into the computerized program are shown in Table1. As Table 1 implies, the electrical properties of tissues in the human body depend on the frequency.

Electric potential distribution by using Eqs. (18)-(20) and its gradients with respect to both axes using Eq. (21) and for *U = 10 [V]* are shown in Fig. 7.

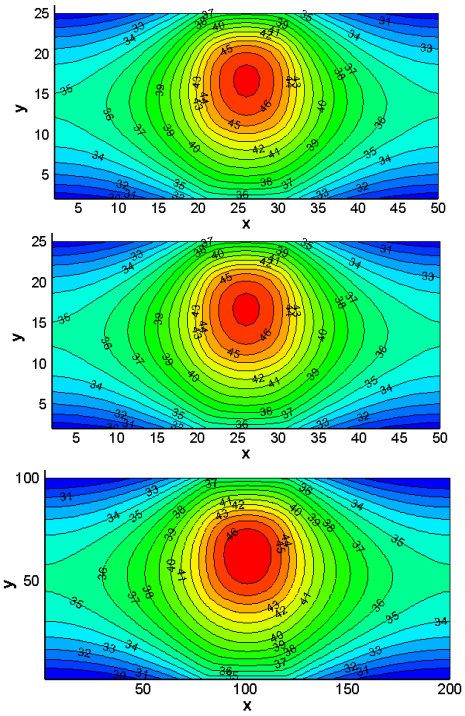

Fig. 4. Independence of the network on the temperature distribution in the tissue (Celsius degrees); (a) $\Delta x = \Delta y = 0.0016m$, (b) $\Delta x = \Delta y = 0.0008\ m$, and (c) $\Delta x = \Delta y = 0.0004\ m$

The results calculated are in agreement with those reported in Ref. [41] except at the points of the edges of the electrodes, because these points have a high gradient. In terms of calculation, due to the limited number of these points, these locations are insignificant and do not have an impact on the temperature results. Temperature distribution for the three modes of *U = 10 [V], f = 10 [MHz]; U = 15 [V], f = 0.1 [MHz]* and *U = 10 [V]*, and *f = 1.0 [MHz]* are obtained by using the Eqs. (23-25) and assuming the convection boundary condition on the skin surface and stable temperature ($h_f = 45\ [W/(m^2K)], T_f = 20$℃). These results are compared in Fig. 8. According to Fig. 8, in the first case, not only much of the tumor is not destroyed by heat, but also the healthy tissues are exposed to damage and high temperature. The second and third modes have better conditions than in the first case. In the second case, although a major part of the tumor is exposed to the high temperature, a large portion of the healthy tissue is also exposed to the high temperature.

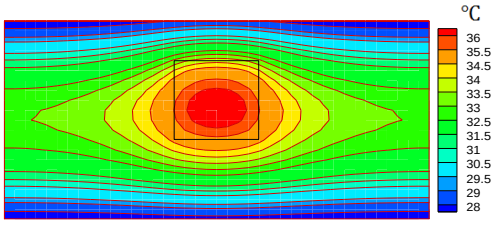

Fig. 5. Temperature distribution in a state of convection on the skin surface.

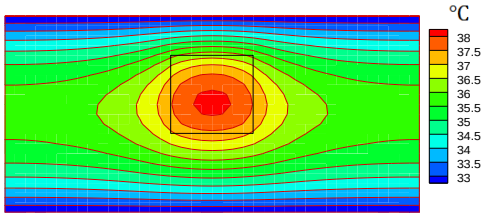

Fig. 6. Temperature distribution in a state of constant temperature on the skin surface.

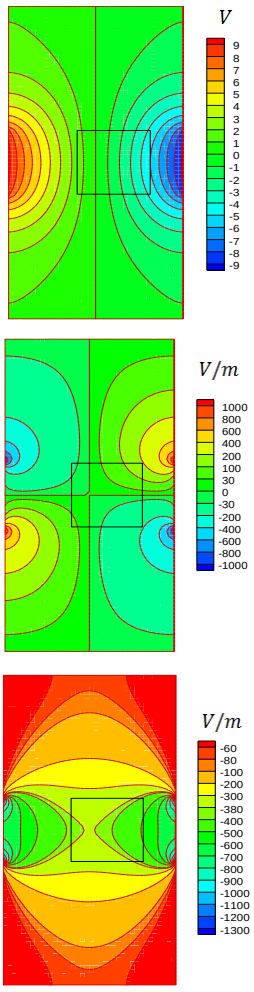

Fig. 7. (a) The potential contours; and its gradients with respect to the (b) x-axis and (c) x-axis.

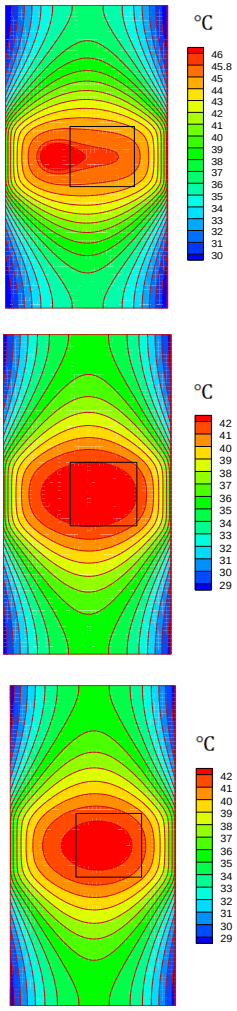

Fig. 8. Temperature distribution in the computing area for (a) first mode ($f = 10\ [MHz], U = 10\ [V]$), (b) second mode ($f = 0.1\ [MHz], U = 15\ [V]$), and (c) third mode ($f = 1.0\ [MHz], U = 10\ [V]$).

Table 1. Electrical properties used in the calculations ($\varepsilon_0 = 8.85 \times 10^{-12} [\mathrm{C}^2/(\mathrm{Nm}^2)$ [41].

Frequency $f[MHz]$	Electrical conductivity $[S/m]$		Dielectric permittivity $[C^2/(Nm^2)]$	
	σ_1	σ_2	ε_1	ε_2
0.1	0.192	1.2 σ_1	20000 ε_0	1.2 ε_1
1.0	0.4	1.2 σ_1	2000 ε_0	1.2 ε_1
10	0.625	1.2 σ_1	100 ε_0	1.2 ε_1

In the third case, despite the high temperature concentrated on the tumor area, a small part of it is heated up to the required temperature. With the conditions governing the issue, damage to the healthy tissues seems unavoidable to achieve appropriate therapeutic results. The results achieved in this section are in agreement with the results achieved in Ref. [41] via the BEM method.

5.1 Model with paramagnetic nanoparticles

In this model, according to the results of the previous section, the magnetic nanoparticles are injected into the tumor area. Other features of this model are similar to that of the previous model. Fig. 9 shows the model.

This problem was studied by Majchrzak and Paruch [30] with BEM and "Inverse problem" to find electric potential, concentration, and radius of nanoparticles, but in the present study the effects of change in all variables containing radius, concentration, susceptibility of nanoparticles, frequency, electric potential, and size of electrodes are investigated. This study is performed by FDM. To validate the results, the assumptions made for the variables are considered as did in Ref. [30]. The result is shown in Fig. 10 for n = 4.8E6, R = 4.2E-8 m. The results are in agreement with each other.

The data on the compound substance composed of the cancerous tissue and magnetic nanoparticles inserted within, assuming a homogeneous distribution, are obtained from Eqs. (11)- (13). Magnetic and thermal properties of magnetic nanoparticles (iron oxide) are as: thermal conductivity coefficient, $K_3 = 40.0\ [W/mK]$; heat capacity, $C_3 = 20.72\ [MJ/m^3K]$; magnetic induction loop radius, $R = 0.01\ [m]$; electrical conductivity, $\sigma_3 = 25000\ [S/m]$; magnetic nanoparticles susceptibility, $\chi'' = 18$.

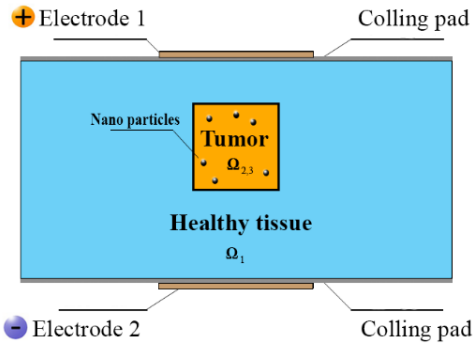

Fig. 9. The studied two-dimensional model and nanoparticles injected within.

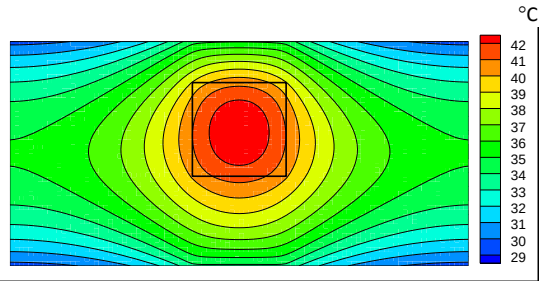

Fig. 10. Temperature distribution in the tissue, $n = 4.8E6, R = 4.2E-8\ m$

According to Eq. (7), the amount of heat generated due to the applied electromagnetic field in healthy tissue is obtained. Also, according to Eq. (8), the amount of heat generated by nanoparticles in tumor tissue is obtained, which is entered into the Pennes equation. Fig. 11 shows the temperature distribution in the tissue with and without magnetic nanoparticles ($h_f = 45\ [W/(m^2K)], T_f = 20$ ℃). According to Fig.11, with the introduction of nanoparticles in the tumor area, not only the temperature increases for around 6°C but also the maximum temperature center focuses in the center of the tumor. Therefore, the use of magnetic nanoparticles leads to energy concentration in the tumor area. With energy-focused within the tumor area, the cancerous tissue is destroyed with minimal damage to the healthy tissues.

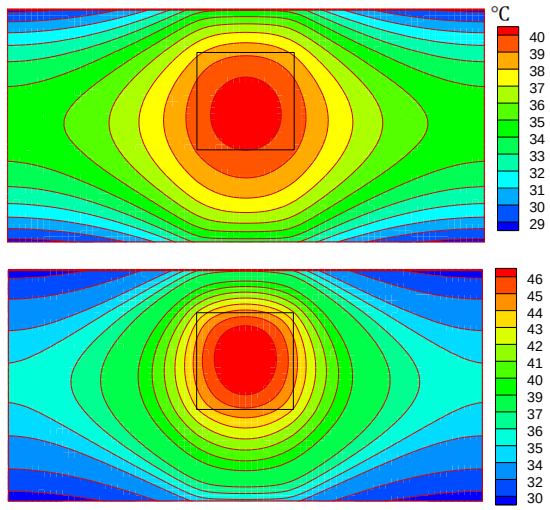

Fig. 11. Temperature distribution in the tissue; (a) without ($U = 8\ V, f = 1\ MHz$) and (b) with ($U = 8\ V, f = 1\ MHz, r = 10\ nm, n = 1E19, \chi'' = 18$) nanoparticles.

To investigate the effect of heating on nanoparticle properties such as density, radius, frequency and the intensity of the electromagnetic field, various modes are considered. The impact of changes in the radius of the nanoparticles and the effect of changes in the concentration of nanoparticles are shown in Fig. 12 and Fig. 13, respectively. With reducing the radius of nanoparticles into half, the temperature greatly reduces so that the temperature increase caused by the use of micro/nanoparticles is only about one degree Celsius. On the other hand, a high increase in the radius of nanoparticles is not possible due to the influence on the magnetic properties [22]. Therefore, an optimal radius should be selected for the particles. With the increment in the concentration of nanoparticles, the maximum temperature within the tumor area rises sharply, while the temperature rise in the vicinity of healthy tissue is low. It should also noted that it is difficult to achieve high concentrations in vitro.

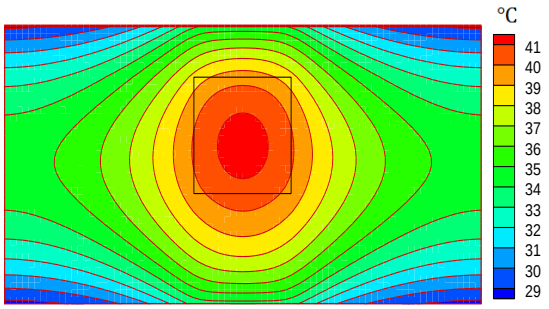

$U = 8\ V, f = 1\ MHz, r = 5\ nm, n = 1E19, \chi'' = 18$

Fig. 12. Impact of change in the radius of the nanoparticles.

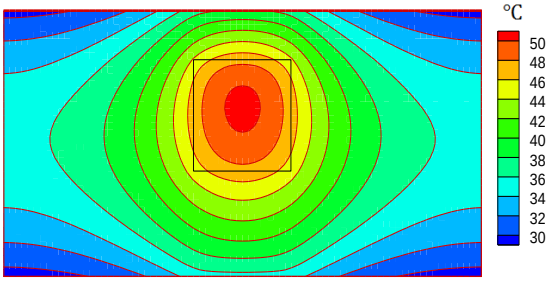

$U = 8\ V, f = 1\ MHz, r = 10\ nm,$ n = 1.5E19, $\chi'' = 18$

Fig. 13. Impact of changes in the concentration of nanoparticles

The impact of changes on magnetic susceptibility and the effect of changes on frequency of the electric field are shown in Fig. 14 and Fig. 15, respectively. With halving the magnetic susceptibility, the maximum temperature is halved. Thus, by changing this quantity, the maximum temperature in the cancerous tissue and normal tissue can be controlled. Increased frequency of the electric field leads to an increased temperature; but this increase in temperature occurs in a wide area of tissues, including the healthy tissue as well. This situation is also observed in the case without the nanoparticles, which is shown in Fig. 8(b).

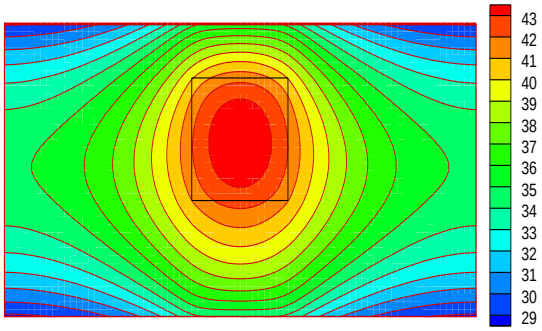

$U = 8\,V, f = 1\,MHz, r = 10\,nm$, n=1E19, $\chi'' = 9$

Fig. 14. Impact of change in susceptibility of nanoparticles.

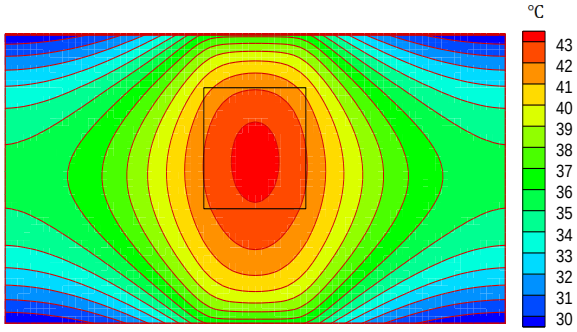

$U = 8\,V, f = 10\,MHz, r = 10\,nm$, n=1E19, $\chi'' = 18$

Fig. 15. Impact of change in frequency of the electric field.

Fig. 16 shows the impact of change in the potential of the electric field. According to this figure, the increased potential difference in the electric field has a huge impact on increasing the temperature of the tumor tissue. With regard to the distribution of temperature, proper determination of this quantity is also helpful in controlling the temperature of the whole tissue area.

The impact of changes in the size of the electrodes is shown in Fig. 17. According to this figure, although the increase in the size of electrodes causes the temperature rise, this temperature increase occurs in a wide area of the tissue. Thus, the risk of injury to the healthy tissues surrounding the cancerous tissue rises.

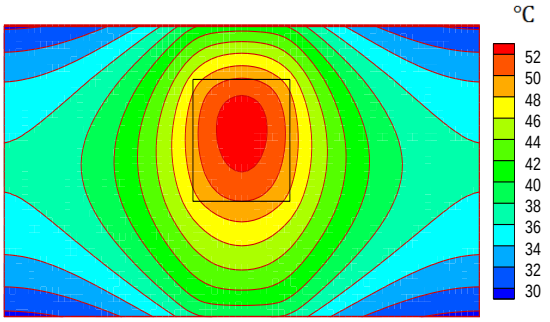

$U = 10\,V, f = 1\,MHz, r = 10\,nm$, n=1E19, $\chi'' = 18$

Fig. 16. Impact of change in the potential of the electric field.

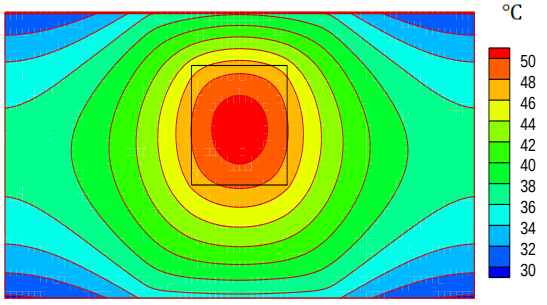

$U = 8\,V, f = 1\,MHz, r = 10\,nm$, n=1E19, $\chi'' = 18$
$\{0.025\,m \le x \le 0.055\,m, y = 0.0\ m\}$
$\{0.025\,m \le x \le 0.055\,m, y = 0.04\,m\}$

Fig. 17. Impact of change in the size of electrodes.

6. Conclusions

The electrical potential has a strong gradient on the edges of the electrodes, which makes it difficult to accurately calculate the gradients.

Changes in the characteristics of the electric field cause changes in the temperature in the entire studied range, while controlling the temperature to maximize it in the center of the tumor through changes in the characteristics of the electric field is quite limited.

Thus, injecting micro/nanoparticles to focus the energy at the center of the tumor is very more promising.

Inserting the micro/nanoparticles into the tumor tissue significantly increases the temperature and cause it to transfer its maximum to the center of the tumor. The major issue is to create high temperature in the tumor tissue while keeping it low in normal tissue around it at the same time. Thus, the properties of micro/nanoparticles should be selected in such a way that the resulting temperature distribution covers such a feature. Through review the results of this study, one can conclude that increasing the radius and concentration of nanoparticles has a positive effect on the temperature distribution. This means that, along with the increase in temperature in the tumor area and the transmission of the maximum temperature to that area, the areas of the healthy tissue will have a negligible increase in temperature. This effect minimizes damage to healthy tissues. However, the optimal radius and accessible concentration in vitro should also be considered. Increasing the size of the electrodes and frequency of the electromagnetic fields have a negative impact, and optimum values must be determined for these quantities. Increasing the frequency of the electric field causes the maximum temperature exit from the center of the tumor and damage the healthy tissues, and increasing the size of the electrodes increases the temperature in a large area of tissue and makes it difficult to control damage to healthy tissues.

Also, due to obtained results, changes in magnetic susceptibility and the electromagnetic field intensity are effective in controlling the temperature in the entire region.

References

[1] R. Cavaliere, E. C. Ciocatto, B. C. Giovanella, C. Heidelberger, R. O. Johnson, M. Margottini, & A. Rossi-Fanelli, A. "Selective heat sensitivity of cancer cells. Biochemical and clinical studies", *Cancer*, Vol. 20, No. 9, pp. 1351-1381, (1967).

[2] J. W. Hand, & G. T. Haar, Heating techniques in hyperthermia. *The British journal of radiology*, Vol. 54, No. 642, pp. 443-466, (1981).

[3] M. Shinkai, "Functional magnetic particles for medical application", *Journal of bioscience and bioengineering*, Vol. 94, No. 6, pp. 606-613, (2002).

[4] P. R. Stauffer, T. C. Cetas, A. M. Fletcher, D. W. Deyoung, M. W. Dewhirst, J. R. Oleson, & R. B. Roemer, "Observations on the use of ferromagnetic implants for inducing hyperthermia", *IEEE Transactions on biomedical engineering*, Vol. 1, pp. 76-90, (1984).

[5] E. Cabuy, "Hyperthermia in Cancer Treatment", *Reliable Cancer Therapies Energy-based therapies*, Vol. 1, No. 2, pp. 1-48, (2011).

[6] M. Urano, & E. B. Douple, (Eds.). *Thermal effects on cells and tissues* (Vol. 1). VSP. (1988).

[7] M. Urano, & E. B. Douple, (Eds.). *Biology of thermal potentiation of radiotherapy* (Vol. 2). VSP. (1989).

[8] M. Urano, & E. B. Douple, (Eds.). *Interstitial hyperthermia: physics, biology and clinical aspects* (Vol. 3). VSP. (1992).

[9] M. Urano, & E. Douple, (Eds). *Chemopotentiation by hyperthermia* (Vol. 4). VSP. (1994).

[10] A. Vander Vorst, A. Rosen, & A. Kotsuka, Y*RF/microwave interaction with biological tissues* (Vol. 181). John Wiley & Sons, (2006).

[11] G. M. Hahn, *Hyperthermia and cancer*. Springer Science & Business Media, (2012).

[12] L. Handl-Zeller, (Ed.). *Interstitial hyperthermia*. Springer Science & Business Media, (2012).

[13 H. I. Robins, J. D. Cohen, & A. J. Neville, *Whole body hyperthermia: biological and clinical aspects*. Springer Science & Business Media, (2012).

[14] S. A. Leibel, & T. L. Phillips, (1998). *Textbook of radiation oncology*. London: WB Saunders, (1998).

[15] R. M. Fratila, & J. M. De La Fuente, *Nanomaterials for Magnetic and Optical Hyperthermia Applications*. Elsevier, (2008).

[16] G. F. Baronzio, & E. D. Hager, (Eds.). *Hyperthermia in cancer treatment: a primer*. Springer Science & Business Media, (2008).

[17] J. C. Lin, & Y. J. Wang, "Interstitial microwave antennas for thermal therapy", *International journal of hyperthermia*, Vol. 3, No. 1, pp. 37-47, (1987).

[18] N. Ikeda, O. Hayashida, H. Kameda, H. Ito, & T. Matsuda, "Experimental study on thermal damage to dog normal brain", *International journal of hyperthermia*, Vol. 10, No. 4, pp.553-561, (1994).

[19] J. Van der Zee, "Heating the patient: a promising approach?", *Annals of oncology*, Vol. 13, No. 8, pp. 1173-1184, (2002).

[20] P. Wust, B. Hildebrandt, G. Sreenivasa, B. Rau, J. Gellermann, H. Riess, & P. M. Schlag, "Hyperthermia in combined treatment of cancer", *The lancet oncology*, Vol. 3, No. 8, pp. 487-497, (2002).

[21] P. Moroz, S. K. Jones, & B. N. Gray, "Status of hyperthermia in the treatment of advanced liver cancer", *Journal of surgical oncology*, Vol. 77, No. 4, pp. 259-269, (2001).

[22] Y. G. Lv, Z. S. Deng, & J. Liu, "3-D numerical study on the induced heating effects of embedded micro/nanoparticles on human body subject to external medical electromagnetic field", *IEEE transactions on nanobioscience*, Vol. 4, No. 4, pp. 284-294, (2005).

[23] M. Sheikholeslami, & M. Seyednezhad, "Simulation of nanofluid flow and natural convection in a porous media under the influence of electric field using CVFEM", *International Journal of Heat and Mass Transfer*, Vol. 120, pp. 772-781, (2018).

[24] M. Sheikholeslami, & A. J. Chamkha, "Flow and convective heat transfer of a ferro-nanofluid in a double-sided lid-driven cavity with a wavy wall in the presence of a variable magnetic field", *Numerical Heat Transfer, Part A: Applications*, Vol. 69, No. 10, pp. 1186-1200, (2016).

[25] M. Sheikholeslami, "Numerical investigation of nanofluid free convection under the influence of electric field in a porous enclosure", *Journal of Molecular Liquids*, Vol. 249, pp. 1212-1221, (2018).

[26] F. Dughiero, & S. Corazza, "Numerical simulation of thermal disposition with induction heating used for oncological hyperthermic treatment", *Medical and Biological Engineering and Computing*, Vol. 43, No. 1, pp.40-46, (2005).

[27] A. Sazgarnia, M. H. Bahreyni Toossi, F. Haji Ghahremani, O. Rajabi, & S. A. Aledavood, "Hyperthermia Effects in the Presence of Gold Nanoparticles Together with Chemotherapy on Saos-2 Cell Line", *Iranian Journal of Medical Physics*, Vol. 8, No. 1, pp. 19-29, (2011).

[28] Q. Zhao, L. Wang, R. Cheng, L. Mao, R. D. Arnold, E. W. Howerth, & S. Platt, "Magnetic nano particle -based hyperthermia for head & neck cancer in mouse models", *Theranostics*, Vol. 2, No. 1, pp. 113-125, (2012).

[29] M. Paruch, "Hyperthermia process control induced by the electric field in order to cancer destroying", *Acta of bioengineering and biomechanics*, Vol. 16, No. 4, (2014).

[30] E. Majchrzak, & M. Paruch, "Application of evolutionary algorithms for identification of number and size of nanoparticles embedded in a tumor region during hyperthermia treatment", *Evolutionary and Deterministic Methods for Design, Optimization and Control with Applications to Industrial and Societal Problems (eds. T. Burczyński and J. Periaux), CIMNE, Barcelona, Spain, A Series of Handbooks on Theory and Engineering Applications of Computational Methods*, pp. 310-315. (2011).

[31] Z. Nemati, J. Alonso, L. M. Martinez, H. Khurshid, E. Garaio, J. A. Garcia, & H. Srikanth, "Enhanced magnetic hyperthermia in iron oxide nano-octopods: size and anisotropy effects", *The Journal of Physical Chemistry C*, Vol. 120, No. 15, pp. 8370-8379, (2016).

[32] C. C. Chen, & J. F. Kiang, "Electroquasistatic Model of Capacitive

Hyperthermia Affected by Heat Convection", *Progress In Electromagnetics Research*, Vol. 89, pp. 61-74. (2019).

[33] M. Coïsson, G. Barrera, C. Appino, F. Celegato, L. Martino, A. P. Safronov, & P. Tiberto, "Specific loss power measurements by calorimetric and thermal methods on γ-Fe2O3 nanoparticles for magnetic hyperthermia", *Journal of Magnetism and Magnetic Materials*, Vol. 473, pp. 403-409, (2019).

[34] Q. Gu, T. Joglekar, C. Bieberich, R. Ma, & L. Zhu, "Nanoparticle Redistribution in PC3 Tumors Induced by Local Heating in Magnetic Nanoparticle Hyperthermia: In Vivo Experimental Study", *Journal of Heat Transfer*, Vol. 141, No. 3, 032402, (2019).

[35] F. Talati, A. A. Taheri "Uncertainty Analysis in Induction Heating by Magnetic Micro/nanoparticles during Hyperthermia", *Tabriz Mechanical Engineering*, Vol. 48, No. 4, pp. 195-201, (2019)

[36] F. Khalighi, A. Ahmadi, & A. Keramat, "Water hammer simulation by explicit central finite difference methods in staggered grids", *Journal of Computational & Applied Research in Mechanical Engineering (JCARME)*, Vol. 6, No. 2, pp. 69-77, (2017).

[37] Y. Cao, Z. Hou, & Y. Liu, (2004). "Finite difference time domain method for band-structure calculations of two-dimensional phononic crystals", *Solid state communications*, Vol. 132, No. 8, pp. 539-543, (2018).

[38] M. Chutia, "Effect of variable thermal conductivity and the inclined magnetic field on MHD plane poiseuille flow in a Porous channel with non-uniform plate temperature", *Journal of Computational & Applied Research in Mechanical Engineering (JCARME)*, Vol. 8, No. 1, pp. 75-84, (2018).

[39] M. Ghalambaz, and A. Noghrehabadi, "Effects of heat generation/absorption on natural convection of nanofluids over the vertical plate embedded in a porous medium using drift-flux model", *Journal of Computational & Applied Research in Mechanical Engineering (JCARME)*, Vol. 3, No. 2, pp. 113-123, (2014).

[40] M. Rahimi, and S. M. Khalafi, "Optimizing naturally driven air flow in a vertical pipe by changing the intensity and location of the wall heat flux", *Journal of Computational & Applied Research in Mechanical Engineering (JCARME)*, Vol. 5, No. 2, pp. 137-145, (2016).

[41] E. Majchrzak, G. Dziatkiewicz, & M. Paruch, "The modelling of heating a tissue subjected to external electromagnetic field", *Acta of Bioengineering and Biomechanics*, Vol. 10, No. 2, pp. 29-37, (2008).

[42] Y. Lv, Y. Zou, & L. Yang, "Theoretical model for thermal protection by microencapsulated phase change micro/nanoparticles during hyperthermia", *Heat and Mass Transfer*, Vol. 48, No. 4, pp. 573-584, (2012).

[43] J. H. Ferziger, & M. Peric, *Computational methods for fluid dynamics*. Springer Science & Business Media, (2012).

How to cite this paper:

Ali Asghar Taheri and Faramarz Talati, "Numerical study of induction heating by micro / nano magnetic particles in hyperthermia ", *Journal of Computational and Applied Research in Mechanical Engineering*, Vol. 9, No. 2, pp. 259-273, (2019).

DOI: 10.22061/jcarme.2019.3961.1465

URL: http://jcarme.sru.ac.ir/?_action=showPDF&article=1022